ACTA ABP BIOCHIMICA POLONICA

Vol. 70, No 2/2023
435–445
https://doi.org/10.18388/abp.2020_6788

Regular paper

Secondary structure in polymorphic forms of alpha-synuclein amyloids

Irena Roterman[1]✉, Katarzyna Stapor[2], Dawid Dułak[3] and Leszek Konieczny[4]

[1]Department of Bioinformatics and Telemedicine, Jagiellonian University, Medical College, Kraków, Poland; [2]Department of Applied Informatics Silesian University of Technology, Gliwice, Poland; [3]ABB Business Services Sp. z o.o. Warszawa, Poland; [4]Chair of Medical Biochemistry, Jagiellonian University, Medical College, Kraków, Poland

Numerous Alpha-synuclein amyloid structures available in PDB enable their comparative analysis. They are all characterized by a flat structure of each individual chain with an extensive network of inter-chain hydrogen bonds. The identification of such amyloid fibril structures requires determining the special conditions imposed on the torsion angles. Such conditions have already been formulated by the Authors resulting in the model of idealised amyloid. Here, we investigate the fit of this model in the group of A-Syn amyloid fibrils. We identify and describe the characteristic supersecondary structures in amyloids. Generally, the amyloid transformation is suggested to be the 3D to 2D transformation engaging mostly the loops linking Beta-structural fragments. The loop structure introducing the 3D organisation of Beta-sheet change to flat form (2D) introduces the mutual reorientation of Beta-strands enabling the large-scale H-bonds generation with the water molecules. Based on the model of idealised amyloid we postulate the hypothesis for amyloid fibril formation based on the shaking, an experimental procedure producing the amyloids.

Keywords: secondary structure, hydrogen bonds, amyloids, alpha-synuclein, polymorphism, 3D structure, 2D structure, air-water interphase, alpha-sheet

Received: 08 April, 2023; revised: 25 May, 2023; accepted: 01 June, 2023; available on-line: 18 June, 2023

✉e-mail: myroterm@cyf-kr.edu.pl

Acknowledgements of Financial Support: This research was partially supported by the European Union's Horizon 2020 programme under Sano No 857533 grant, and the Sano project conducted as part of the International Research Agendas programme of the Foundation for Polish Science. Co-financed by the European Union under the European Regional Development Fund. This research was funded by Jagiellonian University Medical College grant number N41/DBS/000722.

Abbreviations: CC-0,correlation coefficient for starting structures; CC-F, correlation coefficient for residues after elimination of outstanding points; CC-β, correlation coefficient solely for β-structural forms; 2D, 3D, 2-dimensional, 3-dimensional; L-helix, left-handed helix; PDB, Protein Data Bank; RD, Relative Distance;R-helical, right-handed helix

INTRODUCTION

Alpha-synuclein (A-Syn) is a protein whose biological role and structural changes, despite advanced research, remain to be identified (Burré *et al.,* 2018). The mutations in A-Syn are considered as risk conditions (Ottolini *et al.,* 2017; Ghosh *et al.,* 2016). A large spectrum of forms of A-Syn in the context of health and disease is discussed in the paper of Lashuel and others (Lashuel *et al.,* 2013). Post-translational modifications identified in neurodegeneration in patients with Parkinson's disease concern the aggregation propensity of A-Syn (Beyer 2006). A significant contribution of chaperones in the process of A-Syn amyloid transformation is presented in the paper of Burmann (Burmann *et al.,* 2020). There is also a certain degree of synergy between amyloid proteins, including A-Syn and Tau, especially concerning land others iquid-liquid phase separation (Guiney *et al.,* 2020; McDowall *et al.,* 2016). Difficulties in designing therapy arise from the complexity of the amyloid formation mechanism (Dehay *et al.,* 2015; Sivanesam & Andersen 2016). Despite the failure to recognize the amyloid transformation mechanism, analyses of the relationship between structure, function and toxicity are being conducted, focusing on the pathogenesis mechanisms of the synucleopathies phenomenon (Villar-Piqué *et al.,* 2016).

The transformation of A-Syn (described as a 'natively unfolded' monomer adopting an α-helical secondary structure only under the condition of binding to the lipid vesicles) into a highly β-structural one in the amyloid fibril is studied using many experimental techniques: ultracentrifugation, *in vitro* cell-crosslinking and scanning transmission electron microscopy (Bartels *et al.,* 2011). Adopting multivariate conformations identified under diverse conditions, including complexing to nanoscale surfaces, is treated as a potential way of targeting conformational plasticity (D'Onofrio *et al.,* 2020). The A-Syn affinity to the membrane and its ease of interaction is considered a stimulus for therapy design (Bozelli *et al.,* 2020; Kachappilly *et al.,* 2022). The concept of amyloid transformation proposed for prion proteins is also being considered (Lassen *et al.,* 2016.

Concentration-dependent transformation conditions allow the identification of the minimum concentration for fibril production (Afitska *et al.,* 2019). This observation is broadened by research on the impact of various types of interphases on the reaction process, including air-water and hydrophobic surface-water interphases (Ben-Amotz 2022; Schutzius *et al.,* 2015; Yi-Jie & Qu 2014; Eremin & Fokin 2021; Kaplaneris *et al.,* 2022; Ishiyama *et al.,* 2022; Gupta *et al.,* 2022; Cannalire *et al.,* 2022). The possibility of transformation into an amyloid form – thus rich in β-structure – as well as proteins with a high helical structure presence, is surprising in the first stages of these studies (Jayawardena *et al.,* 2017). Another example here may be A-Syn, which in 2/3 of the chain length in the WT form exhibits a helical structure, with the remainder being a loose section with random coil configuration (Ulmer *et al.,* 2005; Tuttle *et al.,* 2016). Considering the breadth of literature on experimental studies, the availability of an increasing number of amyloid structures in PDB resources makes it possible to analyse the structure of amyloid fibrils as such (Goedert *et al.,* 2017; Eisen-

Table 1. Summary of the amyloids A structures discussed in this paper (as available July 20, 2022).
The middle column shows the sections of the A-Syn chain present in a given structure. In the case of superfibrils, the chain identifier is provided, thus indicating the protofibril included in the analysis. *In the case of 2N0A, only the fragment showing the fibrillar form is included.

PDB ID	Fragment	Ref.
7LC9 - F	61-98	(Xiaodan *et al.,* PDB)
6UFR	36-98	(Boyer *et al.,* 2020)]
6A6B -C	37-99	(Li *et al.,* 2018)
6OSJ	37-97	(Ni *et al.,* 2019)
7NCG	37-97	(Lövestam *et al.,* 2021)
6H6B	38-95	(Guerrero-Ferreira *et al.,* 2018)
6FLT	38-95	(Guerrero-Ferreira *et al.,* 2018)
6PEO	36-99	(Boyer *et al.,* 2020)
6PES	36-99	(Boyer *et al.,* 2020)
7NCH	14-25, 36-91	(Ni *et al.,* 2019)
7NCJ	14-25, 36-91	(Ni *et al.,* 2019)
7NCI	14-25, 36-91	(Ni *et al.,* 2019)
6XYO	14-94	(Schweighauser *et al.,* 2020)
6SSX	14-25, 36-91	(Guerrero-Ferreira *et al.,* 2019)
7NCJ	37-97	(Ni *et al.,* 2019)
7NCK	36-99	(Ni *et al.,* 2019)
6XYQ	14-94	(Schweighauser *et al.,* 2020)
6L1U	1-100	(Zhao *et al.,* 2020)
7NCA	37-97	(Ni *et al.,* 2019)
7LC9-A	46-96	(Xiaodan *et al.,* PDB)
6L4S	45-99	(Zhao *et al.,* 2020)
6LRQ	37-99	(Sun *et al.,* 2020)
6CU7	38-97	(Li *et al.,* 2018)
7L7H	36-79	(Hojjatian *et al.,* 2021)
6SST	14-25, 36-96	(Guerrero-Ferreira *et al.,* 2019)
6OSL	39-97	(Li *et al.,* 2018)
6L1T	1-100	(Zhao *et al.,* 2020)
6XYP	14-94	(Schweighauser ???
6OSM	37-96	(Li *et al.,* 2018)
6RTB	9-24, 35-56, 62-93	(Guerrero-Ferreira *et al.,* 2019)
7E0F	50-98	(Sun *et al.,* 2020)
6CU8	43-83	(Li *et al.,* 2018)
6RT0	14-25, 36-97	(Guerrero-Ferreira 2019)
7C1D	46-96	(Sun *et al.,* 2020
2N0A*	30-100	(Tuttle *et al.,* 2016)

berg & Sawaya 2017; Wei *et al.,* 2020). Experiments conducted in different environmental conditions indicate a significant impact on the environment, and therefore, the impact of external conditions (Ben-Amotz 2022; Sawaya *et al.,* 2021; Serpell 2000; Rana *et al.,* 2008; Lambley *et al.,* 2020).

Identification of amyloid fibril structures as consisting of chains with a planar structure requires determining the conditions that should be met in order to obtain just such a form, additionally involving almost all C=O and H-N peptide bond groups in the construction of the hydrogen bond network. Such conditions have already been defined when constructing a model of idealised amyloid (Roterman *et al.*, 2022). The main aim of the present study is to investigate the fulfillment of the conditions formulated for idealised amyloid in the group of A-Syn amyloid fibrils. We also describe the specificity of the secondary structures in amyloids. The primary specificity of amyloid structures is the flatness (2D) of single-chain structures comprising fibrils with a high presence of the β-structure. The combination of several flat-structured chains in the β-form in a parallel chain arrangement makes it possible to engage almost all -N-H and -C=O groups of peptide bonds in the construction of inter-chain hydrogen bonds. Thus, it is possible that each amino acid – in the *i-th* chain – through these groups participates in the construction of two hydrogen bonds (-N-H atoms engaged in the *i-1*-th chain and -C=O group with *i+1*-th chain). It significantly stabilizes the fibril structure, which is observed in experiments. Such engagement is exhibited by amino acids in the helix structure – with H-bonds oriented parallelly and β-structure – with H-bonds oriented antiparallelly. However, globular proteins contain chain fragments in which H-bonds are not generated – like loops and twists in hair-pin structures (Roterman *et al.,* 2022; Roterman 1995). Additionally, the helical form introduces the structure's spatiality (3D), while in theory, the β-structure has the potential of unlimited propagation in a linear form and, in the case of β-sheet, in 2D form as a flat plate. The β-sheet structure – can be generated by different sections of the same chain with different amino acid sequences, while in the amyloid, the β-sheet is formed as a result of a combination of sections of the same sequence originating from many adjacent chains in parallel mutual orientations.

It is shown in this paper that the flat structure of the chain can be reached for β-structural fragments representing special Phi, Psi angles with bends introduced by single R- or L-helical conformation. The identification of such an organisation in polymorphic forms of A-Syn is shown (Peng *et al.,* 2018). Two reference non-amyloid proteins: all-helical and all-β-structural – are also present in the analysis to verify the proposed model.

The role of α-sheet in amyloid construction in comparison to Beta-structural-based amyloids is also discussed (Prosswimmer & Daggett, 2022; Lee *et al.*, 2002; Trexler & Rhoades E. 2012; Balupuri et al. 2019, Milner-White *et al.,* 2006, Hayward & Milner-White 2021). The hypothesis of the external force field of 2D form influence of flat structure construction is presented with the main role of loops linking Beta-structural fragments of chains in native structures of proteins is presented.

Moreover, based on the already proposed model of idealised amyloid we postulate the hypothesis for amyloid fibril formation.

MATERIALS AND METHODS

Data

The structures of A-Syn amyloids (as available in PDB July 2022) analysed in this paper are provided in Table 1.

Two reference proteins are present in the analysis: the GPCR bovine rhodopsin (PDB ID 1GZM – (Li *et al.,* 2004)) mainly Alpha Up-down bundle (CATH classification 1.20.1070.10) representing the structure dominated

by helical form and a FeS cluster assembly protein SufD from *Escherichia coli* (PDB ID 2ZU0 (Wada *et al.,* 2009)) The structure of the second protein is characterised by the presence of large domain build by almost all Beta-structural form.

The torsion angle-based relationship characterizing the amyloid structures

The specificity of amyloid structures is, apart from a high presence of β structure, the flatness of every single chain, a component of the fibrils. The planarity of a polypeptide chain (i.e. its linear propagation) is provided by the rectilinear β-segments (satisfying the Psi=–Phi condition) together with single R-α or L-α helical conformations which introduce a local bend while maintaining a flat structure. Those single helical conformations are characterized by the Psi≈Phi condition. This is why those two characteristics can be put in the common expression |Psi|=|Phi| constituting the basis of the model of idealised amyloid (described in detail in (Roterman *et al.*, 2022).

Quantification of the fit of the idealised amyloid model

The |Psi|=|Phi| relationship of idealised amyloid is assumed here as the hypothetical criterion for amyloid structure identification. The closer to this relationship is the distribution of (Phi, Psi) angles, the more probable the construction of a flat structure.

To enable the assessment of the degree of fit of the idealised amyloid model, the operation of replacing the Phi and Psi values with |Phi| and |Psi| respectively is performed. This leads to a situation where all three lines are in a common position (see the illustration in Figure 3 based on the amyloidogenic fragment (30-100) of the 2N0A).

The degree of fit of chain's (Phi, Psi) angles to the model of idealised amyloid is measured by a Pearson correlation coefficient:

$$C = \frac{\sum_{i=1}^{N}(x_i - \bar{x})(y_i - \bar{y})}{\sqrt{\sum_{i=1}^{N}(x_i - \bar{x})^2}\sqrt{\sum_{i=1}^{N}(y_i - \bar{y})^2}}$$

where x_i stands for $|Phi_i|$ and y_i stands for $|Psi_i|$.

The correlation coefficient CC for the $(|Phi_i|, |Psi_i|)$ angles of residues in an analysed chain was calculated in the following cases:

For all residues in an analysed chain (coefficient marked as CC-0).

For the residues after elimination of outstanding points: i.e. by eliminating them until a value of 0.8 is reached (coefficient marked as CC-F).

For the residues participating in β-strands and satisfying the condition |Psi|=|Phi| with a tolerance of ± 10 deg distance from |Psi|=|Phi| line (coefficient marked as CC-β). Residues with a high CC-F coefficient value are identified as responsible for the stabilization based on a hydrogen bond network.

The described type of analysis will be used to identify the amyloid form providing the maximum proportion of residues with a conformation satisfying the condition |Psi|=|Phi|.

The polypeptide's geometry-based model

This model has already been described on many occasions (see for example Roterman 1995). Here, only the basic assumptions facilitating an interpretation of the discussed results will be recalled. The main idea is to represent the structure of the polypeptide chain using two geometrical parameters. One of them is the curvature radius R which is low and well-defined for the helical structures and very large (theoretically infinitely large) for the β-structures (straight line for certain Phi, Psi angles). The value of the curvature radius is the result of the mutual orientation of two neighbour peptide bond planes expressed by the angle between two peptide bond planes versus the axis defined by virtual Cα-Cα bonds. This angle – called the V-angle – is close to zero (parallel mutual orientation) for helical forms and close to 180 deg for the β-structure (anti-parallel mutual orientation) (Fig. 1). There is one special β-structure with a V-angle=180 deg which produces an ideal straight line (Fig. 1B).

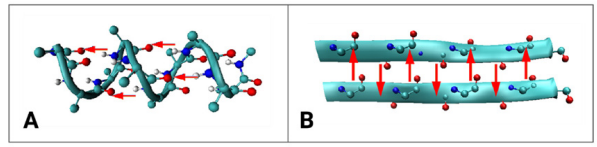

Figure 1. The hydrogen bond system (marked with red arrows): A – parallel in helical form, B – antiparallel in β-structural forms. The arrows just simply visualise the mutual orientations of hydrogen bonds.

Programs used

To visualise the 3D structures of discussed proteins the program VMD was used (https://www.ks.uiuc.edu/Research/vmd/accessed July 2022; Humphrey *et al.,* 1996).

RESULTS

General characteristics of secondary structures in amyloids

In this section, the general characterization of amyloid secondary structures based on the proposed earlier model of idealised amyloid will be presented,

The basic feature of amyloids is the flatness of the structure of single chains that make up the fibril. The planar amyloid structure of each polypeptide chain in a fibril is stabilized by a specific system of hydrogen bonds. In the β-structure with the Psi=–Phi conformation (corresponding to the idealised amyloid), each amino acid participates in the construction of two hydrogen bonds with the adjacent chains. The arrangement of the chains is parallel, which causes residues from corresponding positions from adjacent chains to interact with each other. Such a structure ensures the maximum use of hydrogen bonds, thus providing much stability. Rectilinear chain segments are terminated by single residues with R- or L-helical conformation. A single residue with such a helical conformation does not disturb the planar structure, changing only the turn by introducing a bend (Fig. 2B). The presence of two residues with such a conformation introduces a three-dimensional arrangement disturbing the planarity (Roterman *et al.,* 2022).

Introducing such a single residue with helical conformation results in a change of hydrogen bond ordering. In contrast to a helical structure (which represents a parallel hydrogen bond system – see Fig. 1A), in the ideal β-structure, the arrangement of hydrogen bonds is antiparallel (Fig. 1B). A single residue with the R- or L-helical conformation introduces a local perturbation to this arrangement changing it to a parallel one.

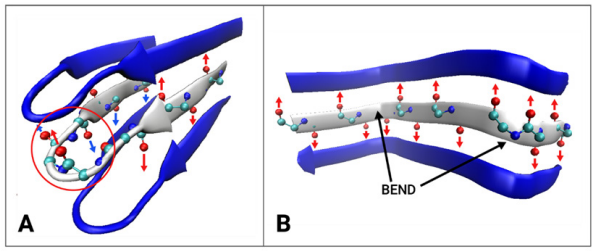

Figure 2. The β-structure propagation:
A – a hair-pin system, B – amyloid. The bend in the form of a hair-pin engages four residues with N-H and O=C groups – H-bonds system locally absent and introduces spaciousness. The one helical residue in the β-structural chain introduces a bend maintaining the flat structure of the chain and additionally continuing the system of H-bonds. The fragment presented in B is the fragment 36-53 of the A-Syn chain in amyloid form (PDB ID 2N0A)

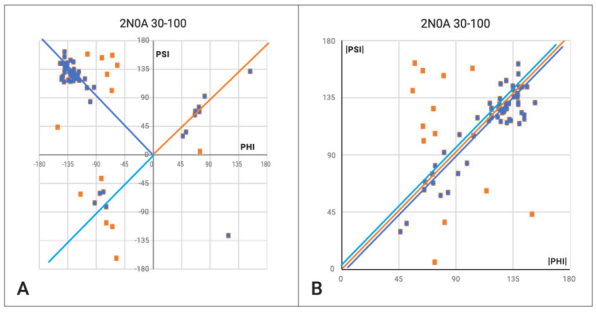

Figure 3. Ramachandran map with the superimposed (Phi, Psi) angles from the A-Syn amyloid (A) and after transformation based on the absolute value of torsion angles (B).
The points representing the residue conformations in the fibrillar sections are marked in navy blue. (30-100 aa).

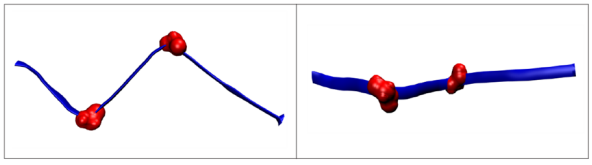

Figure 4. Section 36-53 of the A-Syn chain present in amyloid form (PDB ID 2N0A) in two perspectives.
Residues marked as red – single helical conformations introducing the bend in chain propagation.

The planarity of a polypeptide chain (i.e. its linear propagation) is provided by the rectilinear β-segments (satisfying approximately the Psi=–Phi condition) together with single helical conformations meeting the Psi≈Phi condition (Fig. 4).

In contrast to the above-described structure present in amyloids, changing the turn by means of hair-pins (Fig. 2A) engages more than one residue (most frequently 4 residues) and introduces spatiality. Moreover, the mutual orientation of residues in the hair-pins does not allow the formation of a hydrogen bond system in such bends.

It must be emphasized that the beta-sheet supersecondary structure in amyloids is different from the known, classical structure in other proteins. The classical beta-sheet structures are characterized by a system of hydrogen bonds binding fragments of the same chain. This allows the presence of loops, including the beta-turn (hair-pin) type, which just introduce spatiality. Beta-strand fragments in amyloids remain in one plane due to

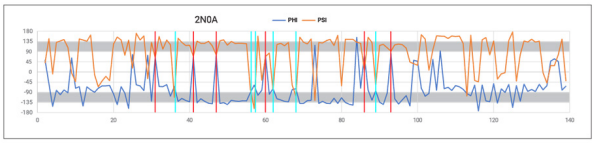

Figure 5. The profiles of Phi (red) and Psi (navy) angles for the complete chain of A-Syn (1-140 aa) (Tuttle *et al.,* 2016).
Grey lines – mark the β conformation fulfilling the Psi=–Phi relation. Vertical lines denote positions of amino acids: red – with L-α conformation, cyan – with R-α conformation. The purpose of this picture is to visualise the differences between 30-100 aa – amyloid fragment to N- and C-terminal fragments, where the Phi, Psi angles relation is significantly different with respect to 30-100 aa fragment.

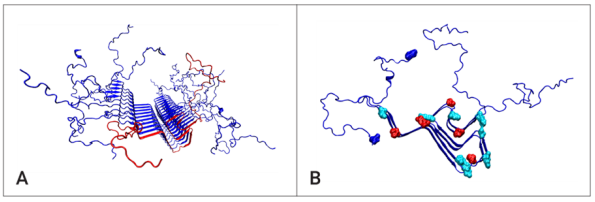

Figure 6. A-Syn structure in the amyloid form (2N0A):
A – the structure of a complete fibril (chain A marked in red); B – two chains with distinguished residues representing the R-α (cyan) and L-α (red) conformation according to the identification provided in Fig. 5.

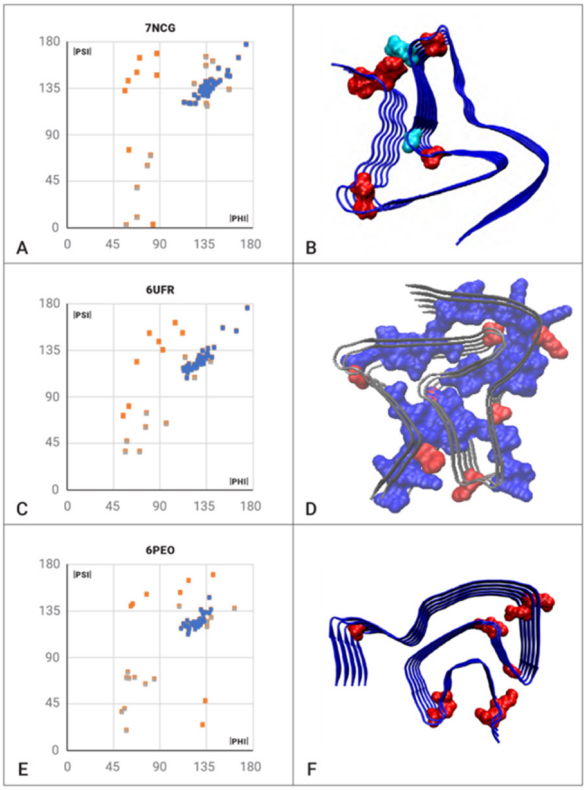

Figure 7. The plot of |Phi| *versus* |Psi| and 3D representation of the discussed amyloids.
The eliminated residues (by CC-F calculations) are marked in red on both the plots and 3D presentation. The points marked in blue – are the positions for residues satisfying the condition |Psi|=|Phi| for β-structural forms. For 6UFR the residues representing the highly ordered β-structural fragments are in space-filling representation (blue).

Table 2. Summary of CC-0 and CC-F values for the set of A-Syn amyloid forms analysed in this paper.
Residue d numbers eliminated in CC-F calculation are given. The CC-β values are given to express the high fulfillment of |Phi| = |Psi| relation. The % of residues in β-structural form for which the CC-β was calculated is given.

PDB ID	CC-0	Residues Eliminated	CC-F	% F	CC-β	% β
7LC9-F	0.815	62, 84	0.851	94	0.922	26.3
6UFR	0.722	69, 74, 85, 87	0.889	93	0.935	69.84
6A6B -C	0.687	74	0.714	98	0.964	15.8
6OSJ	0.636	44, 50, 62, 63	0.799	93	0.952	28.3
7NCG	0.580	59, 69, 84, 87, 93, 94	0.908	90	0.920	63.5
6H6B	0.577	44, 47, 58, 61, 66, 67, 75, 83, 87, 88	0.696	82	0.920	22.4
6FLT	0.564	39, 42, 73, 74, 84, 86	0.777	89	0.909	22.4
6PEO	0.559	42, 60, 61, 68, 72, 73, 85, 86, 87, 97, 98	0.946	82	0.723	63.5
6PES	0.556	42, 72, 73, 85, 87, 97, 98	0.906	89	0.785	59.3
7NCH	0.546	24, 25, 36, 37, 48, 57, 68, 83, 84	0.770	86	0.948	35.3
7NCJ-G	0.544	24, 42, 47, 48, 57, 61, 62, 68, 79, 83, 84	0.849	83	0.908	47.0
7NCI	0.507	24, 25, 36, 37, 42, 48, 57, 61, 62, 68, 78, 79, 83, 84	0.844	79	0.916	38.2
6XYO	0.500	35, 73, 83, 85	0.642	95	0.790	28.4
6SSX	0.464	59, 60, 67 72, 73, 83, 84	0.726	90	0.928	28.7
7NCJ-A	0.451	58, 59, 68, 69, 85, 87, 90, 91	0.882	86	0.829	44.2
7NCK	0.438	43, 58, 68, 72, 74, 85, 87, 97, 98	0.857	86	0.850	45.3
6XYQ	0.436	35, 37, 42, 73, 83, 88	0.610	92	0.862	25.9
6L1U	0.435	9, 10, 24, 47, 60, 83, 99	0.616	93	0.954	20.0
7NCA	0.400	51, 52, 58, 59, 68, 69, 85, 87, 90, 91	0.909	83	0.885	55.7
7LC9-A	0.394	50, 51, 66, 67, 76	0.730	88	0.0.962	33.3
6L4S	0.390	50, 53, 54, 67, 72, 74, 80, 84, 90	0.679	83	0.902	30.9
6LRQ	0.372	38, 41, 46, 58, 68, 72, 85, 87, 97, 98	0.790	84	0.909	25.4
6CU7	0.367	39, 40, 67, 68, 69, 83, 84,86, 90	0.665	85	0.916	26.6
7L7H	0.363	40, 44, 76	0.501	93	0.954	11.3
6SST	0.357	59, 60, 67, 72, 73, 83, 84	0.715	90	0.910	28.7
6OSL	0.334	43, 50, 60, 65, 66, 84, 85, 93, 94, 95	0.697	83	0.944	27.1
6L1T	0.327	3, 22, 29, 30	0.606	96	0.945	13.0
6XYP	0.310	15, 35, 37, 43, 53, 73, 74, 83, 86,	0.612	88	0.937	16.0
6OSM	0.276	38, 42, 50, 51, 52, 77, 84, 89, 94	0.626	85	0.937	20.0
6RTB	0.220	13, 36, 52, 55, 67, 68, 69, 74, 86, 87, 88	0.613	84	0.911	22.8
7E0F	0.202	52, 65, 72, 74, 79, 80, 84	0.507	85	0.894	24.4
6CU8	0.200	44, 50, 65, 67, 68	0.540	87	0.812	26.3
6RT0	0.163	43, 67, 72, 73, 83, 84, 91	0.691	90	0.888	27.3
7C1D	0.152	50, 60, 67, 72, 73, 76, 77, 83, 85, 87	0.480	80	--	1.9
2N0A (30-100)	0.528	32, 33, 34, 36, 57, 58, 59, 80, 85, 86, 87, 98	0.899	83	0.847	45.0

a turn introduced by a single R- or L-helical conformations as shown in Fig. 4. Such a radical turn allows the chain to propagate in one plane.

Figure 4 visualises the real conformation present in 36-53 fragment of A-Syn which appears to be almost ideally accordant with the proposed model of idealised amyloid. Linear propagation of β-structural fragments with single residues representing helical conformation results in a flat form with well-defined bends. The orientation of hydrogen bonds in β-fragments is antiparallel with local, parallel orientation in single helical residues.

Analysis of the fit of the idealised amyloid model 2N0A protein

In this section, the procedure of fitting the idealised amyloid model will be presented based on the reference A-Syn amyloid structure (2N0A – section 36-53). In Fig. 4, the fragments of the chain (marked as navy blue) show a rectilinear system obtained using the Phi and Psi torsion angles satisfying the relation Psi=–Phi. The residues marked in red have an α-helix conformation resulting in a turn of the chain while maintaining its flatness.

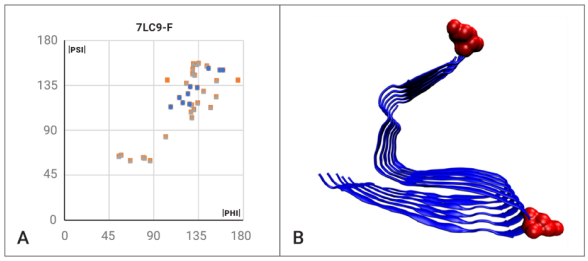

Figure 8. Presentation of the 7LC9-F amyloid with the highest CC-0 value (and the lowest number of outstanding residues).
A – distribution of points representing |Phi| and |Psi|. Only two residues are considered outstanding (red points). Their location in the chain is highlighted in red (space-filling) on the 3D representation (B).

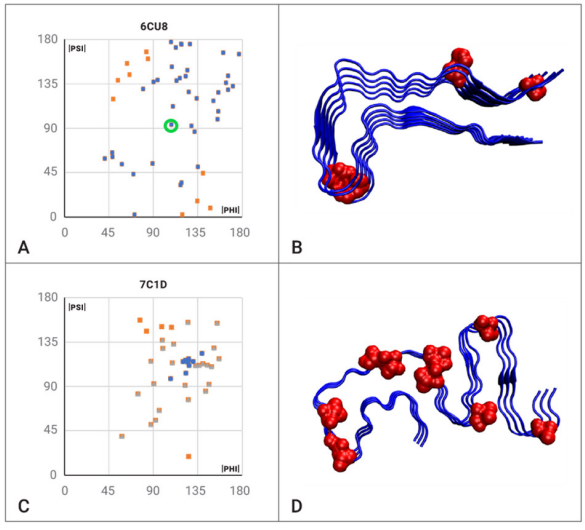

Figure 9. Examples with low CC values:
A – CC-0 – all points; CC-F blue points; The circled dot is the only point satisfying the |Psi|=|Phi|. C – red points eliminated for CC-F calculation, gray points – CC-F calculation, blue points – CC-β calculation. B, D – 3D presentation of 6CU8 and 7C1D respectively with red residues – residues eliminated for CC-F calculation

The torsion angle profiles of the mentioned fragment are shown in Fig. 5. The fulfillment of relations Psi=–Phi is visible for the amyloid part (positions 30-100 aa), which is marked in gray. Within the clearly ordered and constant values of the Phi and Psi angles for the β form, single positions with the Phi and Psi angles corresponding to the R (cyan) and L (red) helical conformations are visible. The visualization of structures In this analysis is shown in Fig. 6.

Analysis of the structure of A-Syn amyloid forms

Table 2 provides the CC-0 and CC-F values of the chain as described in the Materials and Methods section. The values of CC-β express the status of residues satisfying the condition |Psi|=|Phi| in relation solely to the β-structural form. The % of residues satisfying the condition for CC-β is also given to characterise the degree of the presence of such restrictive structure in a particular protein.

Figure 9 shows examples with high values of CC-0 and CC-F arising from the location of the Phi and Psi angles in accordance with the Psi=-Phi relationship. In a 3D visualization, these sections are represented by a rectilinear arrangement. The highlighted residues – red points – on the plots of |Phi| and |Psi| angles are residues treated as outstanding, the elimination of which results in a CC-F value > 0.8 (Table 2).

In the amyloid with PDB code 7NCG, the rectilinear β-structure sections are visible (Fig. 7B) and the corresponding locations of the |Phi|*versus*|Psi| plot (Fig. 7A). Items that do not satisfy the |Psi|=|Phi| condition specified by the model are marked in red. The number of residues that do not satisfy the model is low and they do not disturb the overall form of this amyloid leaving it close to the principles of the proposed model.

A similar arrangement is identified in the case of 6URF (Fig. 7). It should be noted that this structure is characterised only by a few residues with conformations not satisfying model conditions.

The significant portion of a chain in 6PEO amyloid meets the |Psi|=|Phi| condition, but a fairly significant scattering of several residues deviating from the model can also be observed.

The highest CC-0 value and the low number of residues deviating from the model are characteristic for amyloid 7LC9-F (Fig. 8). Eliminating only two residues results in a very high value of CC-F=0.851.

Further examples are the structures present in 6CU8 and 7C1D exhibiting the lowest CC-0 values (Fig. 9). In these two examples, no rectilinear propagation, but rather an "undulating" form is observed. This means, that the chain propagation is composed of sections with a smaller radius R. This reduction of radius applies to short sections, which, with an alternating arrangement similar to the R- and L-helical conformations, does not result in a spatial form. In this case, the hydrogen bonding arrangement is not parallel, although the deflection from the perpendicularity to the chain's plane is compensated, resulting in maintaining the structure's flatness.

Analysis of the structure of reference examples

Two reference proteins (Table 3) represent mainly helical and β-structural proteins. As shown in Fig. 10 their structure is highly ordered. The FeS cluster assembly of SufD from *Escherichia coli* is a protein which for the most part shows the β-structure (Banach *et al.,* 2020). The analysed fragment of this protein is limited to the beta-sheets (Fig. 10B).

The parallel orientation in the β-sheet (Fig. 10B) indicates a structural similarity to amyloids. However, the sequential β-strands represent a different sequence, while in amyloids the sequences in all neighbouring chains are identical.

The status expressed by CC-β of sequential β-strands and β-sheets reveals differences with respect to the amyloid forms discussed (Table 4). The fragments showing high accordance with the |Psi|=|Phi| criterion (having high CC values) are accompanied by the fragments with completely opposite characteristics (low CC val-

Table 3. Characteristics of the reference proteins

PDB ID	NAME	CC-0	CC-F	CC-β	%
2ZU0	FeS cluster	0.297	0.803	0.949	28.4
1GZM	rhodopsin	0.334	0.803	0.970	2.4

Table 4. Status (CC- β) of β-strands in β-sheets (as distinguished in Fig. 10B).
The values in parentheses – denote the β-strand status for the residues representing non-β-structural Phi, Psi angles. The values given for β-sheets are calculated only for the residues belonging to the β-structural area on the Ramachandran map.

β-sheet - red		β-sheet - blue	
FRAGMENT	CC-β	FRAGMENT	CC-β
181-192	0.860 (0.501)	167-176	0.613
211-219	0.290	196-206	0.876 (0.361)
239-246	0.700	225-234	–0.012 (-0.477)
266-273	0.010	251-260	0.642 (0.263)
295-304	0.020	280-291	0.833
327-337	0.712	309-318	–0.374
357-364	0.587	341-351	–0.064
β-sheet	0.641	β-sheet	0.511

ues). The non-β-structural conformations are present in the selected fragments (values given in parentheses in Table 4). Visual analysis of two β-sheets suggests the perfect β-structural organisation (Fig. 11). However, the analysis of Phi and Psi angles reveals some residues in the lower left quarter of the Ramachandran map. Some β-strands having torsion angles typical for β-structure appear to be not organised as expected in amyloids. The differentiation of β-strands can be observed. The status of sequential β-strands in the amyloid is identical for all fragments belonging to a common β-sheet. The distribution of |Psi|, |Phi| angles (Fig. 12A) identifies the large number of points satisfying the |Psi|=|Phi| relation, however, it also shows their dispersion over the chain. The highest similarity is observed in the 181-192 fragment (marked in Fig. 12B).

The mainly-helical protein is difficult to evaluate with the |Phi|=|Psi| criterion due to the very low presence of β-structural conformations. The distribution of Phi, Psi angles along the chain (Fig. 13) shows high accordance with the helical forms (dark lines on Fig. 13). The CC-0 for this protein is equal to 0.347, the CC-F=0.807 (the eliminated residues marked as blue dots – Fig. 13.). The number of eliminated residues constitutes 19.2% of the whole length of the chain. The linear relation between torsion angles is mostly due to the Psi≈Phi relation present in the helical conformation.

The eliminated amino acids (in the CC-F calculations) represent the unstructured fragments like loops particularly those external with respect to the surrounding membrane. The space filling presentation (Fig. 12C and 12D) distinguishes the segments satisfying to a large extent the |Psi|=|Phi| relation, however, they belong mostly to the helical region.

The proposed hypothetical mechanism of amyloid fibril formation

The proposed hypothesis of amyloid fibril formation presented here concerns the method and the reasons of the transformation of a 3D structure into a planar form characteristic to the amyloid structures.

We also want to refer here to the existing, different hypothesis ((Prosswimmer & Daggett, 2022; Lee *et al.*, 2002; Trexler & Rhoades, 2012; Balupuri *et al.*, 2019) of the formation of the amyloid based on the α-sheet structure as an intermediate in the aggregation process.

Shaking an aqueous solution of proteins as a laboratory technique for obtaining amyloid forms of proteins consists in increasing the presence of air-water interphase in the solution. Such a shaking process can simulate the conditions in a cell of a living organism. The air-water interphase has a surface structure, so it introduces an external force field with 2D characteristics.

Occasionally, a protein undergoes some conformational changes resulting in aggregation competent polypeptide chain. Such a chain, avoiding contact with air strives for maximum contact with water, which is available only on one side. The most thermodynamically favora-

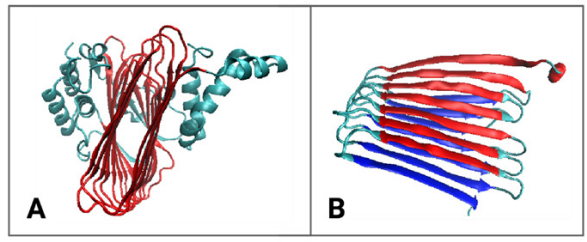

Figure 10. 3D structure 2ZU0
A – chain A – with two β-sheets marked in red. B – two β-sheets marked in red and blue – N-terminal residue – marked with space filling.

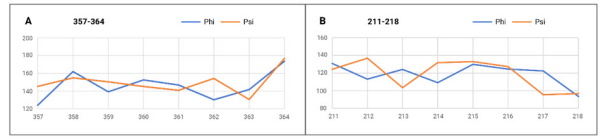

Figure 11. Phi, Psi profiles in the fragment with high (A) and low (B) correlation according to Table 4.

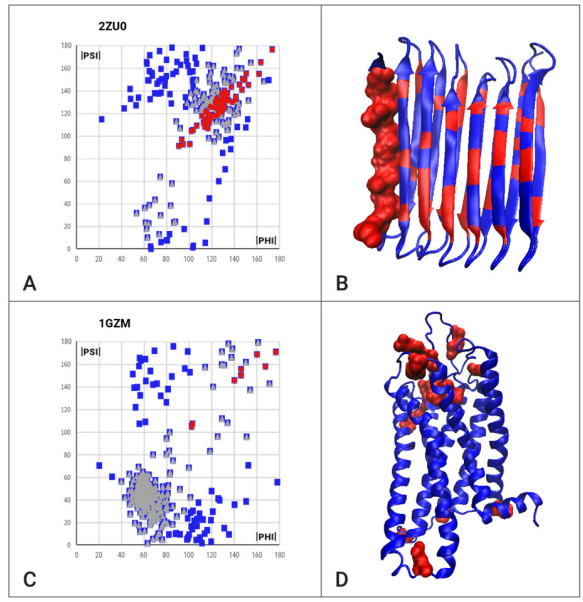

Figure 12. Characteristics of all-β and all-helical proteins.
A – |Phi|, |Psi| angles as they appear in the β-structural part of the protein – chain fragment selected as an aim-oriented example for the analysis of the beta-structural form of the chain. B – 3D presentation with conformations satisfying the relation |Psi|=|Phi| – red. The space-filling – a fragment of the highest satisfaction of |Psi|=|Psi| condition. C – |Phi|, |Psi| angles as they appear in all-helical protein. D – 3D structure with amino acids satisfying the |Psi|=|Phi| conditions distinguished by a space-filling presentation. The red dots – all |Phi|, |Psi| angles to calculate CC-0, grey dots – CC-F and red – CC-β. The same colours are used in 3D presentation (red and blue).

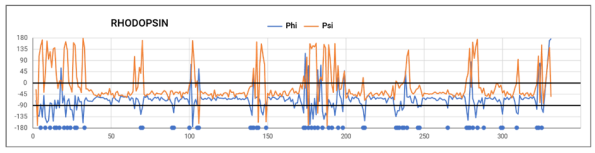

Figure 13. Profiles of Phi and Psi angles in rhodopsin.
The black lines mark the range for the helical structure to visualise the closeness to the Psi=Phi relation for helical fragments. Positions not satisfying this relation are marked by blue dots on the x-axis.

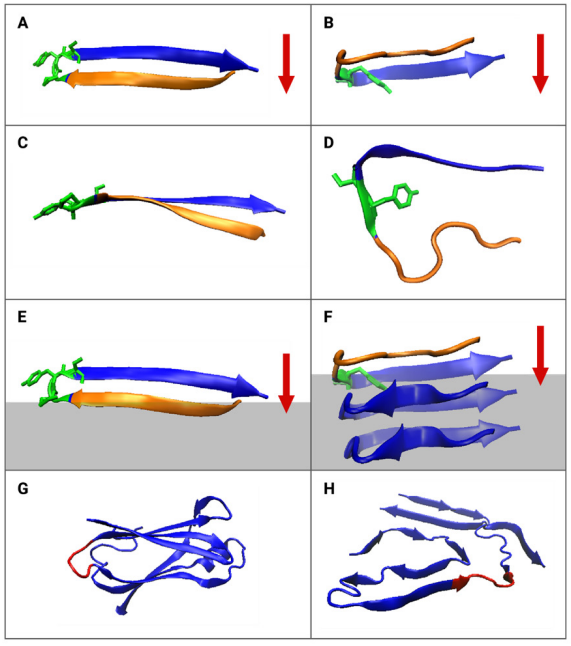

Figure 14. Structure of the transthyretin:
A, C– native form 104-125 fragment of transthyretin – green fragment loop 113-115 – different orientation – orange – residues 104 - 112. B, D – amyloid form 104-125 fragment of transthyretin – green fragment loop 113-115, orange residues – fragment 104-112. E – as in A with water phase shown in gray with orange fragment in contact with a water phase. F – as in B with water phase shown in gray – complete chain in contact with water. G – native form of transthyretin – red fragment loop 97-103. H - amyloid form of transthyretin – red fragment loop 97-103. The orientation in A, B, E and F figures is as follows: the H-bonds (red arrows) system is perpendicular to the plane of the water surface. The gray area – water, white area – air. The green fragment – the loop causing the propagation of the chain in 3D space in native form and in 2D space in the amyloid form. The red arrow crossed out on D – the H-bonds system between two fragments of the same polypeptide chain is not present. The groups participating in H-bonds are oriented perpendicularly to the paper plane on C and D.

ble situation is the formation of a system of hydrogen bonds with a planar chain where the polypeptide chain "lies" on the water surface. In this way, the backbone chain engages as many C=O and N-H groups of peptide bonds as possible in such an interaction. This explains the reason for the almost planar form of the chain in amyloid fibril.

A planar polypeptide chain formed due to the shaking finds a thermodynamically favorable opportunity to interact with another planar chain and the process of attaching the next flat chains continues until the aggregation nucleus is formed. The next phase starting from the nucleus is characterized by a rapid formation of fibrils composed of beta-sheet structures.

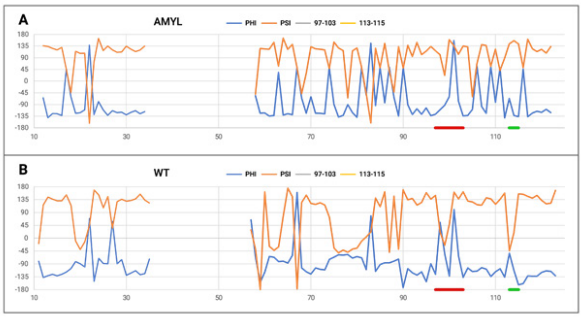

Figure 15. Profiles of Phi and Psi angles for the amyloid and WT forms of transthyretin with highlighted fragments responsible for changing the orientation of the chain propagation as shown in Fig. 14.

Amyloid transformation mainly requires conformational changes within the loops that change from 3D orientation to 2D one.

The influence of the environment on amyloid transformation with an unchanged sequence is widely recognized (Serpell, 2000). The particular form of the environment in the form of mentioned 2D interphase seems to favour the formation of the flat structure of the chains – components of amyloid fibrils.

The proposed hypothesis for amyloid fibril formation is illustrated in Fig. 14. It refers to the transthyretin (Ueda, 2022) which undergoes amyloid transformation relatively easily. A special object is a fragment of a beta-sheet identified as A (11-19), G(104-112) and H (114-124). Both the WT form (PDB ID 1DVQ (Klabunde *et al.,* 2000) and the amyloid form (PDB ID 6SDZ (Schmidt *et al.,* 2019)) are available in PDB. Another reason is the possibility to compare with the hypothesis proposed in the works (Prosswimmer & Daggett, 2022, Armen *et al.,* 2004) and based on α-sheet structure as intermediate.

Fragment beta-strand A(11-19) remains in this form in range (13-15), fragment G (104-112) changes its form to a disordered linearly propagating segment, while fragment H (114-124) remains in beta form on (118-124) fragment. The shortening of beta-stand segments can be observed.

The water-directed beta-structural fragment 104-111 can form hydrogen bonds with water molecules. The shape of the loop directs the second part of the beta-strand above the water surface, i.e. to the air zone. This is due to the orientation imposed by the loop (113-115) present in the native form of the transthyretin (green fragment in Fig. 14A and C). The same fragment after changing the conformation of the loop results in a planar structure of the entire fragment 104-124 (green fragment in Fig. 14B and D).

It should be noted that the native Beta-structure segment (104-112) changes its form to a disordered pattern, while the native-form beta-structure segment (114-124) is limited to the amyloid segment (118-124). This means that the conformational change within the loop (green fragment in Fig. 14A–D) also applies to a short fragment of the Beta-ordered segment. As a result of these changes, the structure of the entire fragment 104-124 becomes planar, allowing the generation of hydrogen bonds with water molecules along its entire length (Fig. 14E and F). The same analysis applies to loops 97-103 (Fig. 14G and H), where a change in conformation within the loop (red fragment Fig. 14G and H) allows backbone contact

(groups -C=O and -N-H of peptide bonds) with water molecules leading to the formation of hydrogen bonds with water molecules. The exact conformation changes within the discussed loops are shown in Fig. 15.

The proposed amyloid formation hypothesis relies on the 3D to 2D transformation engaging mostly the loops linking beta-structural fragments. The loops structure introducing the 3D organisation of beta-sheet change to a flat form introducing the mutual reorientation of beta-strands enabling the generation of large-scale hydrogen bonds initially with water molecules to change into an inter-chain H-bonds system in the next step.

The α-sheet structure, widely discussed in the context of amyloids (Prosswimmer & Daggett, 2022; Lee *et al.,* 2002; Trexler & Rhoades, 2012; Balupuri *et al.,* 2019) is the structure formed by amino acids with the R- and L-helical conformations alternating in the polypeptide chain. Similarly to the Beta-sheet structure, the α-sheet structure is characterized by the rectilinear form (Fig. 2 in Prosswimmer & Daggett, 2022). The distribution of Phi and Psi angles in α-sheet structures discussed in Prosswimmer & Daggett (2022) is consistent with the model assumed in this work. The difference is only quantitative. In the case of the α-sheet, the concentration of points on the Ramachandran map is significantly greater in the positions corresponding to the R- and L-helix with the presence of the Phi and Psi angles representing the β-structure in a linear relationship. In the current work, for the β forms, a much greater concentration of points on the Ramachandran map is observed. The main point is concentrated on the 3D to 2D transition. The structure discussed in (Prosswimmer & Daggett, 2022) introduces the 3D structuralisation which is not present in amyloid formation. The linear propagation of the chain in the form of Beta is the most frequently observed secondary form. The linear propagation of the chain is also possible in the form of R- followed by L-helix by turns. Such a system allows the generation of an H-bonds network. The mutual orientation of chains shall be parallel to allow propagation in fibril formation. However, the flat construction for individual chain is the most important one.

DISCUSSION

The amyloid structure of the flat form of each polypeptide chain is stabilized by a specific hydrogen bond arrangement. Each amino acid in an idealized form contributes to the construction of two hydrogen bonds with adjacent chains. The chain arrangement is parallel, causing identical residues to interact with each other in adjacent chains. The maximum use of C=O and H-N groups for the construction of hydrogen bonds is ensured by the β-structure with the Psi=–Phi conformation. A rectilinear form with C=O groups facing in the opposite direction to the H-N group of the same amino acid is an arrangement that makes maximum use of the possibilities of the hydrogen bonding structure. The rectilinear sections are terminated by single residues with R-α or L-α conformations. A single residue with such conformation does not disturb the flat structure, only changing the direction (introduction of a turn/bend). In this case, the form of arranging hydrogen bonds is changed. In a structure with the Psi=–Phi conformation, the hydrogen bond arrangement perpendicular to the plane of the chain represents an anti-parallel arrangement (if a turn is applied to the hydrogen bond).

Numerous amyloid forms of A-Syn allow tracking the structural variation of these amyloids. Among the structures satisfying the |Psi|=|Phi| condition, there are structures showing some deviations from this condition. The deviation also provides fibrillar structures.

On the Ramachandran map presenting the distribution of radius of curvature R and V-angle (Roterman *et al.,* 2022; Roterman, 1995) the area fulfilling the Psi=–Phi condition represents the one with the highest value of R (i.e. a straight chain section). A reduction of the curvature radius R is observed moving up and down versus this line gradually introducing the arc form. If this procedure is performed stepwise (i.e. one above the Psi=–Phi line followed by one representing Phi, Psi angles below that line), this introduces the structural form as shown in Fig. 9 for 7C1D (symmetrically located |Psi|, |Phi| angles). The result of such Phi, Psi angle combination is the sinusoidal arrangement of the chain as can be seen in 7C1D (Fig. 9) and others. The local introduction of an arc-like form in one direction is compensated by an ark form oriented in the opposite direction. In consequence, the linear propagation of the flat form can be continued. Nevertheless, this symmetrical (with respect to |Phi|=|Psi| line) set of altered Phi and Psi angles generates a flat arrangement, but probably with reduced stabilization derived from the hydrogen bonds (change of angle between the C=O and H-N groups in the hydrogen bonding arrangement of peptide bonds derived from adjacent polypeptides).

The condition of the presence of an R- or L-helical conformation at the turn of the chain can be satisfied in a less perfect form by a conformation with a low curvature radius R. Cyan and red lines in Fig. 5 and Fig. 6 illustrate the area with low values of V-angle and the R-radius of curvature. The presence of Phi and Psi angles from this area satisfies the condition for obtaining a turn, although the hydrogen bond arrangement is not as perfectly ordered as in the case of Phi and Psi angles accurately representing the R-α- or L-α-helical conformation.

The phenomenon of polymorphism in the case of amyloids is conditioned by environmental factors, as indicated by numerous experimental studies (Ben-Amotz, 2022; Schutzius *et al.,* 2015; Zuo & Qu 2014; Eremin & Fokin, 2021; Kaplaneris *et al.,* 2022; Ishiyama *et al.,* 2022; Gupta *et al.,* 2022; Cannalire *et al.,* 2022; Jayawardena *et al.,* 2017; Ulmer *et al.,* 2005; Tuttle *et al.,* 2016).

This analysis complements the detailed structural analysis of A-Syn fibrils (Roterman *et al.,* 2023) as well as the transthyretin (Roterman *et al.,* 2022), where the characteristics of fibrils were considered from the perspective of the tertiary structure and characteristics of those fibrils. Microenvironmental conditions were also indicated as the cause of structural changes in A-Syn (Candelise *et al.,* 2020; Stephens *et al.,* 2019).

The problem of describing the field in the form of 3D analyzed on a large-scale provides many forms of mathematical notation to express its presence (Cheng *et al*., 2023).

CONCLUSIONS

The flat structure of single chains – components of amyloid fibril – is a characteristic of amyloid forms. This flatness is achieved through a β-type structure satisfying the Psi=–Phi condition resulting in a rectilinear chain propagation. Turns in chain arrangement are obtained by single residues with R-α or L-α helical conformation

(satisfying Psi≈Phi condition). The combination of such β-structures and single conformations allows the introduction of the general model expressed by |Psi|=|Phi|. The hypothesis introduced in this paper is to treat the presence of conformations satisfying this relation as a criterion for amyloid identification and description. The stabilization of such a form is achieved through the special hydrogen bond arrangement. In β-structured sections, the hydrogen bond arrangement is antiparallel. Each individual residue of the L-α or R-α conformation introduces a local arrangement of these bonds as parallel. Access to multiple structural forms of A-Syn amyloids reveals variation in the form of this ordering. This variation is likely a result of different environmental conditions (Roterman *et al.,* 2023). Particularly, the impact of the presence of air-water interphase (increasing this presence during shaking) is most likely indicated as a factor affecting the structuring, including the form of arranging the hydrogen bond network in amyloids.

External conditions in the form of air-water interphase also direct protein structuring to the planar form, which can be stabilized by a significantly high number of hydrogen bonds of -N-H and -C=O groups of peptide bonds. The accessibility of these groups for hydrogen bonds also includes segments that in their native form represent loops introducing 3D structuring (e.g. two parallel β-sheets) resulting in a flat structure for the entire polypeptide chain (Fig. 14G and H).

Declarations

Acknowledgements. Many thanks to Anna Śmietańska and Zdzisław Wiśniowski for technical support.

Conflicts of Interest. The authors declare no conflict of interest

REFERENCES

Afitska K, Fucikova A, Shvadchak VV, Yushchenko DA (2019) α-Synuclein aggregation at low concentrations. *Biochim Biophys Acta Proteins Proteom* **1867**: 701–709. https://doi.org/10.1016/j.bbapap.2019.05.003

Armen RS, DeMarco ML, Alonso DOV, Daggett V (2004) Pauling and Corey's α-pleated sheet structure may define the prefibrillar amyloidogenic intermediate in amyloid disease. *Proc Natl Acad Sci U S A* **101**: 11622–11627. https://doi.org/10.1073/pnas.0401781101

Balupuri A, Choi KE, Kang NS (2019) Computational insights into the role of α-strand/sheet in aggregation of α-synuclein. *Sci Rep* **9**: 59. https://doi.org/10.1038/s41598-018-37276-1.

Banach M, Konieczny L, Roterman I (2020) Anti-amyloid drug design. In *From globular proteins to amyloids*. pp 215–232. Elsevier

Bartels T, Choi JG, Selkoe DJ (2011) α-Synuclein occurs physiologically as a helically folded tetramer that resists aggregation. *Nature* **477**: 107–110. https://doi.org/10.1038/nature10324

Ben-Amotz D (2022) Electric buzz in a glass of pure water. *Science* **376**: 800–801. https://doi.org/10.1126/science.abo3398

Beyer K (2006) Alpha-synuclein structure, posttranslational modification and alternative splicing as aggregation enhancers. *Acta Neuropathol* **112**: 237-251. https://doi.org/10.1007/s00401-006-0104-6

Boyer DR, Li B, Sun C, Fan W, Zhou K, Hughes MP, Sawaya MR, Jiang, Eisenberg DS (2020) The α-synuclein hereditary mutation E46K unlocks a more stable, pathogenic fibril structure. *Proc Natl Acad Sci U S A* **117**: 3592–3602. https://doi.org/10.1073/pnas.1917914117

Bozelli JC Jr, Kamski-Hennekam E, Melacini G, Epand RM (2021) α-Synuclein and neuronal membranes: Conformational flexibilities in health and disease. *Chem Phys Lipids* **235**: 105034. https://doi.org/10.1016/j.chemphyslip.2020.105034

Burmann BM, Gerez JA, Matečko-Burmann I, Campioni S, Kumari P, Ghosh D, Mazur A, Aspholm EE, Šulskis D, Wawrzyniuk M, Bock T, Schmidt A, Rüdiger SGD, Riek R, Hiller S (2020) Regulation of α-synuclein by chaperones in mammalian cells. *Nature* **577**: 127–132. https://doi.org/10.1038/s41586-019-1808-9

Burré J, Sharma M, Südhof TC (2018) Cell biology and pathophysiology of α-Synuclein. *Cold Spring Harb Perspect Med* **8**: a024091. https://doi.org/10.1101/cshperspect.a024091.

Candelise N, Schmitz M, Thüne K, Cramm M, Rabano A, Zafar S, Stoops E, Vanderstichele H, Villar-Pique A, Llorens F, Zerr I (2020) Effect of the micro-environment on α-synuclein conversion and implication in seeded conversion assays. *Transl Neurodegener* **9**: 5. https://doi.org/10.1186/s40035-019-0181-9.

Cannalire R, Santoro F, Russo C, Graziani G, Tron GC, Carotenuto A, Brancaccio D, Giustiniano M (2022) Photomicellar catalyzed synthesis of amides from isocyanides: optimization, scope, and NMR Studies of photocatalyst/surfactant interactions. *ACS Organic Inorganic Au* **2**: 66–74. https://doi.org/10.1021/acsorginorgau.1c00028

Cheng X, Fan Z, Yao S, Jin T, Lv Z, Lan Y, Bo R, Chen Y, Zhang F, Shen Z, Wan H, Huang Y, Zhang Y (2023) Programming 3D curved mesosurfaces using microlattice designs. *Science* **379**: 1225–1232. https://doi.org/10.1126/science.adf3824

Chiti F, Dobson CM (2017) Protein misfolding, amyloid formation, and human disease: a summary of progress over the last decade. *Annu Rev Biochem* **86**: 27–68. https://doi.org/10.1146/annurev-biochem-061516-045115

Dehay B, Bourdenx M, Gorry P, Przedborski S, Vila M, Hunot S, Singleton A, Olanow CW, Merchant KM, Bezard E, Petsko GA, Meissner WG (2015) Targeting α-synuclein for treatment of Parkinson's disease: mechanistic and therapeutic considerations. *Lancet Neurol* **14**: 855–866. https://doi.org/10.1016/S1474-4422(15)00006-X

D'Onofrio M, Munari F, Assfalg M (2020) Alpha-synuclein-nanoparticle interactions: understanding, controlling and exploiting conformational plasticity. *Molecules* **25**: 5625. https://doi.org/10.3390/molecules25235625

Eisenberg DS, Sawaya MR (2017) Structural studies of amyloid proteins at the molecular level. *Annu Rev Biochem* **86**: 69–95. https://doi.org/10.1146/annurev-biochem-061516-045104

Eremin DB, Fokin VV (2021) On-water selectivity switch in microdroplets in the 1,2,3-triazole synthesis from bromoethenesulfonyl fluoride. *J Am Chem Soc* **143**: 8374–18379. https://doi.org/10.1021/jacs.1c08879

Ghosh D, Mehra S, Sahay S, Singh PK, Maji SK (2017) α-synuclein aggregation and its modulation. *Int J Biol Macromol* **100**: 37–54. https://doi.org/10.1016/j.ijbiomac.2016.10.021

Goedert M, Eisenberg DS, Crowther RA (2017) Propagation of Tau aggregates and neurodegeneration. *Annu Rev Neurosci* **40**: 189–210. https://doi.org/10.1146/annurev-neuro-072116-031153

Guerrero-Ferreira R, Taylor NM, Arteni A-A, Kumari P, Mona D, Ringler P, Britschgi M, Lauer ME, Makky A, Verasdonck J, Riek R, Melki R, Meier BH, Böckmann A, Bousset L, Stahlberg H (2019) Two new polymorphic structures of human full-length alpha-synuclein fibrils solved by cryo-electron microscopy. *Elife* **8**: e48907. https://doi.org/10.7554/eLife.48907

Guerrero-Ferreira R, Taylor NM, Mona D, Ringler P, Lauer ME, Riek R, Britschgi M, Stahlberg H (2018) Cryo-EM structure of alpha-synuclein fibrils. *Elife* **7**: e36402. https://doi.org/10.7554/eLife.36402

Guiney SJ, Adlard PA, Lei P, Mawal CH, Bush AI, Finkelstein DI, Ayton S (2020) Fibrillar α-synuclein toxicity depends on functional lysosomes. *J Biol Chem* **295**: 17497–17513. v10.1074/jbc.RA120.013428

Gupta A, Vankar JK, Jadav JP, Gururaja GN (2022) Water mediated direct thioamidation of aldehydes at room temperature. *J Organic Chem* **87**: 2410–2420. https://doi.org/10.1021/acs.joc.1c02307

Hayward S, Milner-White EJ (2021) Determination of amino acids that favour the α_l region using Ramachandran propensity plots. Implications for α-sheet as the possible amyloid intermediate. *J Struct Biol* **213**: 107738. https://doi.org/10.1016/j.jsb.2021.107738

Hojjatian A, Dasari AKR, Sengupta U, Taylor D, Daneshparvar N, Yeganeh FA, Dillard L, Michael B, Griffin RG, Borgnia M, Kayed R, Taylor KA, Lim KH (2021) Distinct cryo-Em structure of alpha-Synuclein filamen derived by tau. *BioRxiv* Preprint. https://doi.org/https://doi.org/10.1101/2020.12.31.424989

https://www.ks.uiuc.edu/Research/vmd/accessed July 2022

Humphrey W, Dalke A, Schulten K (1996) VMD: visual molecular dynamics. *J Mol Graph* **14**: 27–28, 33–38. https://doi.org/10.1016/0263-7855(96)00018-5

Ishiyama T, Tahara T, Morita A (2022) Why the photochemical reaction of phenol becomes ultrafast at the air-water interface: the effect of surface hydration. *J Am Chem Soc* **144**: 6321–6325. https://doi.org/10.1021/jacs.1c13336

Jayawardena N, Kaur M, Nair S, Malmstrom J, Goldstone D, Negron L, Gerrard JA, Domigan LJ (2017) Amyloid fibrils from hemoglobin. *Biomolecules* **7**: 37. https://doi.org/10.3390/biom7020037

Kachappilly N, Srivastava J, Swain BP, Thakur P (2022) Interaction of alpha-synuclein with lipids. *Methods Cell Biol* **169**: 43–66. https://doi.org/10.1016/bs.mcb.2021.12.002

Kaplaneris N, Vilches-Herrera M, Wu J, Ackermann L (2022) Sustainable ruthenium(II)-catalyzed C–H activations in and on H_2O. *ACS Sust Chem Engin* **10**: 6871–6888. https://doi.org/10.1021/acssuschemeng.2c00873

Klabunde T, Petrassi HM, Oza VB, Raman P, Kelly JW, Sacchettini JC (2000) Rational design of potent human transthyretin amyloid disease inhibitors. *Nat Struct Biol* **7**: 312–321. https://doi.org/10.1038/74082

Lambley H, Schutzius TM, Poulikakos D (2020) Superhydrophobic surfaces for extreme environmental conditions. *Proc Natl Acad Sci U S A* **117**: 27188–27194. https://doi.org/10.1073/pnas.2008775117

Lashuel HA, Overk CR, Oueslati A, Masliah E (2013) The many faces of α-synuclein: from structure and toxicity to therapeutic target. *Nat Rev Neurosci* **14**: 38–48. https://doi.org/10.1038/nrn3406

Lassen LB, Reimer L, Ferreira N, Betzer C, Jensen PH (2016) Protein partners of α-synuclein in health and disease. *Brain Pathol* **26**: 389–397. https://doi.org/10.1111/bpa.12374

Lee H-J, Shin SY, Choi C, Lee YH, Lee S-J (2002) Formation and removal of alpha-synuclein aggregates in cells exposed to mitochondrial inhibitors. *J Biol Chem* **277**: 5411–5417. https://doi.org/10.1074/jbc.M105326200

Li B, Ge P, Murray KA, Sheth P, Zhang M, Nair G, Sawaya MR, Shin WS, Boyer DR, Ye S, Eisenberg DS, Zhou ZH, Jiang L (2018) Cryo-EM of full-length α-synuclein reveals fibril polymorphs with a common structural kernel. *Nat Commun* **9**: 3609. https://doi.org/10.1038/s41467-018-05971-2

Li J, Edwards PC, Burghammer M, Villa C, Schertler GFX (2004) Structure of bovine rhodopsin in a trigonal crystal form. *J Mol Biol* **343**: 1409–1438. https://doi.org/10.1016/j.jmb.2004.08.090

Li Y, Zhao C, Luo F, Liu Z, Gui X, Luo Z, Zhang X, Li D, Liu C, Li X (2018) Amyloid fibril structure of α-synuclein determined by cryo-electron microscopy. *Cell Res* **28**: 897–903. https://doi.org/10.1038/s41422-018-0075-x

Long H, Zheng W, Liu Y, Sun Y, Zhao K, Liu Z, Xia W, Lv S, Liu Z, Li D, He K-W, Liu C (2021) Wild-type α-synuclein inherits the structure and exacerbated neuropathology of E46K mutant fibril strain by cross-seeding. *Proc Natl Acad Sci U S A* **118**: e2012435118. https://doi.org/10.1073/pnas.2012435118

Lövestam S, Schweighauser M, Matsubara T, Murayama S, Tomita T, Ando T, Hasegawa K, Yoshida M, Tarutani A, Hasegawa M, Goedert M, Scheres SHW (2021) Seeded assembly *in vitro* does not replicate the structures of α-synuclein filaments from multiple system atrophy. *FEBS Open Bio* **11**: 999–1013. https://doi.org/10.1002/2211-5463.13110

McDowall JS, Brown DR (2016) Alpha-synuclein: relating metals to structure, function and inhibition. *Metallomics* **8**: 385–397. https://doi.org/10.1039/c6mt00026f

Milner-White JE, Watson JD, Qi G, Hayward S (2006) Amyloid formation may involve alpha- to beta sheet interconversion *via* peptide plane flipping. *Structure* **14**: 1369–1376. https://doi.org/10.1016/j.str.2006.06.016

Ni X, McGlinchey RP, Jiang J, Lee JC (2019) Structural insights into α-synuclein fibril polymorphism: effects of Parkinson's disease-related C-terminal truncations. *J Mol Biol* **431**: 3913–3919. https://doi.org/10.1016/j.jmb.2019.07.001

Ottolini D, Calí T, Szabò I, Brini M (2017) Alpha-synuclein at the intracellular and the extracellular side: functional and dysfunctional implications. *Biol Chem* **398**: 77–100. https://doi.org/10.1515/hsz-2016-0201

Peng C, Gathagan RJ, Lee VM (2018) Distinct α-Synuclein strains and implications for heterogeneity among α-Synucleinopathies. *Neurobiol Dis* **109**(Pt B): 209–218. https://doi.org/10.1016/j.nbd.2017.07.018

Prosswimmer T, Daggett V (2022) The role of α-sheet structure in amyloidogenesis: characterization and implications. *Open Biol* **12**: 220261. https://doi.org/10.1098/rsob.220261

Rana A, Gupta TP, Bansal S, Kundu B (2008) Formation of amyloid fibrils by bovine carbonic anhydrase. *Biochim Biophys Acta* **1784**: 930–935. https://doi.org/10.1016/j.bbapap.2008.02.020

Roterman I, Stapor K, Dulak D, Konieczny L (2022) The Possible mechanism of amyloid transformation based on the geometrical parameters of early-stage intermediate in silico model for protein folding. *Int J Mol Sci* **23**: 9502. https://doi.org/10.3390/ijms23169502

Roterman I, Stapor K, Konieczny L (2023) Structural specificity of α-synuclein amyloid. *Biomedicines* **11**: 1324. https://doi.org/10.3390/biomedicines11051324

Roterman I (1995) Modelling the optimal simulation path in the peptide chain folding – studies based on geometry of alanine heptapeptide. *J Theor Biol* **177**: 283–288. https://doi.org/10.1006/jtbi.1995.0245

Sawaya MR, Hughes MP, Rodriguez JA, Riek R, Eisenberg DS (2021) The expanding amyloid family: Structure, stability, function, and pathogenesis. *Cell* **184**: 4857–4873. https://doi.org/10.1016/j.cell.2021.08.013

Schmidt M, Wiese S, Adak V, Engler J, Agarwal S, Fritz G, Westermark P, Zacharias M, Fändrich M (2019) Cryo-EM structure of a transthyretin-derived amyloid fibril from a patient with hereditary ATTR amyloidosis. *Nat Commun* **10**: 5008. https://doi.org/10.1038/s41467-019-13038-z

Schutzius TM, Jung S, Maitra T, Graeber G, Köhme M, Poulikakos D (2015) Spontaneous droplet trampolining on rigid superhydrophobic surfaces. *Nature* **527**: 82–85

Schweighauser M, Shi Y, Tarutani A, Kametani F, Murzin AG, Ghetti B, Matsubara T, Tomita T, Ando T, Hasegawa K, Murayama S, Yoshida M, Hasegawa M, Scheres SHW, Goedert M (2020) Structures of α-synuclein filaments from multiple system atrophy. *Nature* **585**: 464–469. https://doi.org/10.1038/s41586-020-2317-6

Serpell LC (2000) Alzheimer's amyloid fibrils: structure and assembly. *Biochim Biophys Acta* **1502**: 16–30. https://doi.org/10.1016/s0925-4439(00)00029-6

Siegert A, Rankovic M, Favretto F, Ukmar-Godec T, Strohäker T, Becker S, Zweckstetter M (2021) Interplay between tau and α-synuclein liquid-liquid phase separation. *Protein Sci* **30**: 1326–1336. https://doi.org/10.1002/pro.4025

Sivanesam K, Andersen NH (2016) Modulating the Amyloidogenesis of α-Synuclein. *Curr Neuropharmacol* **14**: 226–237. https://doi.org/10.2174/1570159x13666151030103153

Stephens AD, Zacharopoulou M, Kaminski Schierle GS (2019) The cellular environment affects monomeric α-synuclein structure. *Trends Biochem Sci* **44**: 453–466. https://doi.org/10.1016/j.tibs.2018.11.005

Sun Y, Hou S, Zhao K, Long H, Liu Z, Gao J, Zhang Y, Su X-D, Li D, Liu C (2020) Cryo-EM structure of full-length α-synuclein amyloid fibril with Parkinson's disease familial A53T mutation. *Cell Res* **30**: 360–362. https://doi.org/10.1038/s41422-020-0299-4

Sun Y, Long H, Xia W, Wang K, Zhang X, Sun B, Cao Q, Zhang Y, Dai B, Li D, Liu C (2021) The hereditary mutation G51D unlocks a distinct fibril strain transmissible to wild-type α-synuclein. *Nat Commun* **12**: 6252. https://doi.org/10.1038/s41467-021-26433-2

Trexler AJ, Rhoades E (2012) N-Terminal acetylation is critical for forming α-helical oligomer of α-synuclein. *Protein Sci* **21**: 601–605. https://doi.org/10.1002/pro.2056

Tuttle MD, Comellas G, Nieuwkoop AJ, Covell DJ, Berthold DA, Kloepper KD, Courtney JM, Kim JK, Barclay AM, Kendall A, Wan W, Stubbs G, Schwieters CD, Lee VMY, George JM, Rienstra CM (2016) Solid-state NMR structure of a pathogenic fibril of full-length human α-synuclein. *Nat Struct Mol Biol* **23**: 409–415. https://doi.org/10.1038/nsmb.3194

Ueda M (2022) Transthyretin: Its function and amyloid formation. *Neurochem Int* **155**: 105313. doi: 10.1016/j.neuint.2022.105313

Ulmer TS, Bax A, Cole NB, Nussbaum RL (2005) Structure and dynamics of micelle-bound human alpha-synuclein. *J Biol Chem* **280**: 9595–9603. https://doi.org/10.1074/jbc.M411805200

Villar-Piqué A, Lopes da Fonseca T, Outeiro TF (2016) Structure, function and toxicity of alpha-synuclein: the Bermuda triangle in synucleinopathies. *J Neurochem* **139** (Suppl 1): 240–255. https://doi.org/10.1111/jnc.13249

Wada K, Sumi N, Nagai R, Iwasaki K, Sato T, Suzuki K, Hasegawa Y, Kitaoka S, Minami Y, Outten FW, Takahashi Y, Fukuyama K (2009) Molecular dynamism of Fe-S cluster biosynthesis implicated by the structure of the SufC(2)-SufD(2) complex. *J Mol Biol* **387**: 245–258. https://doi.org/10.1016/j.jmb.2009.01.054

Wei Z, Li Y, Cooks RG, Yan X (2020) Accelerated reaction kinetics in microdroplets: overview and recent developments. *Annu Rev Phys Chem* **71**: 31–51. https://doi.org/10.1146/annurev-physchem-121319-110654

Xiaodan N, Ryan PM, Jiansen J, Jennifer CL (2021) Cryo-EM structure of the N-terminal alpha-synuclein truncation 41-140. *Proc Natl Acad Sci U S A* **118**: (35) e2023487118. https://doi.org/10.1073/pnas.202348711

Zhao K, Li Y, Liu Z, Long H, Zhao C, Luo F, Sun Y, Tao Y, Su X-D, Li D, Li X, Liu C (2020) Parkinson's disease associated mutation E46K of α-synuclein triggers the formation of a distinct fibril structure. *Nat Commun* **11**: 2643. https://doi.org/10.1038/s41467-020-16386-3

Zhao K, Lim Y-J, Liu Z, Long H, Sun Y, Hu J-J, Zhao C, Tao Y, Zhang X, Li D, Li Y-M, Liu C (2020) Parkinson's disease-related phosphorylation at Tyr39 rearranges α-synuclein amyloid fibril structure revealed by cryo-EM. *Proc Natl Acad Sci U S A* **117**: 20305–20315. https://doi.org/10.1073/pnas.1922741117

Zuo Y-J, Jin Qu (2014) How does aqueous solubility of organic reactant affect a water-promoted reaction?. *J Organic Chem* **79**: 6832–6839. https://doi.org/10.1021/jo500733v